ROYAL SOCIETY OF CHEMISTRY

Check for updates

Unraveling the timescale of the structural photo-response within oriented metal–organic framework films†

Sumea Klokic, [a] Denys Naumenko,[a] Benedetta Marmiroli,[a] Francesco Carraro, [b] Mercedes Linares-Moreau, [b] Simone Dal Zilio,[c] Giovanni Birarda, [d] Rupert Kargl,[e] Paolo Falcaro [b] and Heinz Amenitsch [*a]

Fundamental knowledge on the intrinsic timescale of structural transformations in photo-switchable metal–organic framework films is crucial to tune their switching performance and to facilitate their applicability as stimuli-responsive materials. In this work, for the first time, an integrated approach to study and quantify the temporal evolution of structural transformations is demonstrated on an epitaxially oriented **DMOF-1**-on-MOF film system comprising azobenzene in the **DMOF-1** pores (**DMOF-1/AB**). We employed time-resolved Grazing Incidence Wide-Angle X-Ray Scattering measurements to track the structural response of the **DMOF-1/AB** film upon altering the length of the azobenzene molecule by photo-isomerization (*trans*-to-*cis*, 343 nm; *cis*-to-*trans*, 450 nm). Within seconds, the **DMOF-1/AB** response occurred fully reversible and over several switching cycles by cooperative photo-switching of the oriented **DMOF-1/AB** crystallites as confirmed further by infrared measurements. Our work thereby suggests a new avenue to elucidate the timescales and photo-switching characteristics in structurally responsive MOF film systems.

Introduction

Stimuli-responsive materials change their properties as an immediate response towards an external trigger and have attracted great attention for their technological applicability as actuators, sensors or storage systems.[1–3] The key to their outstanding functional versatility arises from their structure, which comprises the proper relationship between crystallinity and flexibility.[4–6] A prominent example of stimuli-responsive materials is metal–organic frameworks (MOFs),[6–10] which are built by a highly ordered porous network of metal ions and organic linker molecules, where both constituents allow chemically tuning of the flexibility of the framework's backbone.[6,7,11–13] The structural response of most flexible MOFs can be reversibly triggered by a chemical or physical stimulus,[8,14] which led to the ever-growing class of switchable MOFs.[13,15,16]

aInstitute of Inorganic Chemistry, Graz University of Technology, 8010 Graz, Austria. E-mail: heinz.amenitsch@tugraz.at

bInstitute of Physical and Theoretical Chemistry, Graz University of Technology, 8010 Graz, Austria

cIOM-CNR, Laboratorio TASC, S.S. 14, 163.5 km, Basovizza, Trieste 34149, Italy

dElettra Sincrotrone Trieste – SISSI Bio Beamline, S.S. 14, 163.5 km, Basovizza, Trieste 34149, Italy

eInstitute of Chemistry and Technology of Bio-Based Systems, Graz University of Technology, 8010 Graz, Austria

† Electronic supplementary information (ESI) available. See https://doi.org/10.1039/d2sc02405e

Herein, the term 'switchable' refers to MOFs that undergo a substantial and reversible change in the unit cell dimensions under the full retention of the framework's connectivity and crystallinity,[10] as it was shown by molecular simulations exemplarily for MIL-53(Al),[17] DMOF-1 (ref. 11) or CAU-13.[18] Although the chemistry and the related design strategies regarding stimuli-responsive MOFs is enormously rich in the literature,[6–9,13,19–21] little is known about the temporal response characteristics of the MOF structure towards the incoming stimulus.[3,7,22] Yet, only by understanding the MOF response over the time course of its stimuli-induced switch, the design of MOF systems with the desired response kinetics becomes feasible.[22,23] This idea of controlling the intrinsic timescale of dynamic structural transformations in MOFs has recently led to the concept of four-dimensional MOFs (4D-MOFs).[22] In 4D-MOFs, the time-axis is considered as the fourth dimension and represents the temporal evolution of a stimuli-induced structural transformation in a flexible MOF system. As pointed out by Evans *et al.*,[22] Ehrling *et al.*[16] and Haldar *et al.*,[3] an open challenge is the design of switchable MOF systems with precise temporal responses. However, we note that this goal can only be achieved by the development of a methodological approach that elucidates the time-axis of the structural response in light-responsive MOF systems.

It has been recently outlined in numerous reviews that amongst the flexible MOFs,[3,8,20,22,24] especially for photo-switchable MOF film systems the structural dynamics remain

largely unexplored,[25–28] which is mainly because the MOF films employed in previous studies were structurally non-responsive.[25,29–33]

In this work, we demonstrate the example of a photo-switchable, azobenzene infiltrated **DMOF-1/AB** film system (**DMOF-1** = Zn$_2$BDC$_2$DABCO, BDC = terephthalic acid, DABCO = 1,4-diazabicyclo[2.2.2]octane; AB = azobenzene),[28,34–36] and that the photo-triggered temporal response of the **DMOF-1/AB** structure can be deliberately accelerated by 3 orders of magnitude simply by choosing the oriented MOF-on-MOF film-fabrication strategy[37–39] over the bulk system.[34] The oriented film growth is ensured by matching the lattice constants of the upper **DMOF-1** structure with the lower Cu$_2$BDC$_2$-on-Cu(OH)$_2$ MOF layer,[37,38] where the latter is grown in a first step with its (001) plane oriented parallel to the glass substrate.[38,40,41] The absorption of ultraviolet light provokes the infiltrated azobenzene molecule[3,36,42] in the **DMOF-1** pores[34,43] to isomerize between its *trans*-to-*cis* configuration (ON), whilst visible light triggers the reversed *cis*-to-*trans* transition (OFF).[3,8,44] Our findings show that within seconds this photo-induced isomerization process forces the **DMOF-1** film structure to adapt,[28,34,42a] thus switching between the ON and OFF state. Yet, although various techniques have been demonstrated to monitor the stimuli-induced structural response over time in switchable bulk MOF systems, such as spectroscopy,[23,45] X-ray diffraction[46] and similar ones,[47] there is still an open quest for experimental techniques which are applicable for MOF film structures.[16] To this aim, we herein further report a methodological approach to study the photo-switching behavior of the **DMOF-1/AB** film system by time-resolved Grazing Incidence Wide Angle X-Ray Scattering (GIWAXS) using synchrotron radiation in combination with laser irradiation sources.[48] Moreover, GIWAXS is a powerful tool for real-time monitoring of the structural responses where both, the **DMOF-1/AB** film surface and the buried Cu$_2$BDC$_2$-on-Cu(OH)$_2$ layer can be resolved with high resolution.[49] Hence, based on GIWAXS and infrared spectroscopic data, we found that the azobenzene isomerization channels the entire **DMOF-1/AB** film in a cooperative lattice movement[16,50] to adapt to the size of the infiltrated azobenzene molecule and demonstrate that this ON and OFF behavior of the **DMOF-1/AB** film is fully reversible over several cycling repetitions.

To the best of our knowledge, an oriented MOF film which undergoes a photo-induced switch of both the azobenzene and the MOF-cage, as defined in this study, has not been reported so far. The great interest in photo-switchable MOFs is mainly because light is arguably one of the most attractive stimuli,[21] as it provokes non-destructively the material's response which can be remotely controlled over certain distances.[8,26,33,51] Hence, characterizing the timescale of dynamic transitions in photo-switchable MOF films will especially aid in their development for applications[21,30,42] in sensing,[52] energy storage[28] or cargo uptake and release.[21,53]

Results and discussion

The procedure for the fabrication of the **DMOF-1**-on-MOF film system is illustrated in Fig. 1(a). The lower MOF layer comprises

the oriented Cu$_2$BDC$_2$ structure grown on the Cu(OH)$_2$ nanobelt film, which is fabricated by following the secondary hetero-epitaxial growth strategy[38] based on an automated nanobelt deposition procedure.[41] The subsequent **DMOF-1** growth occurs by matching its crystal lattice with the lower Cu$_2$BDC$_2$-on-Cu(OH)$_2$ layer (Fig. 1(b and c))[38] and is obtained by following a two-step method: Firstly, the Zn(acetate)$_2$ nodes are covalently attached to the loose carboxylate groups of the Cu$_2$BDC$_2$-on-Cu(OH)$_2$ layer, which is then followed by converting the film in a methanolic linker solution (H$_2$BDC = terephthalic acid, DABCO = 1,4-diazabicyclo[2.2.2]octane). Thusly, the hetero-epitaxial Cu$_2$BDC$_2$ MOF film was used for the fabrication of the oriented **DMOF-1** system by following the MOF-on-MOF approach.[40a] The orientation of the fabricated **DMOF-1** film system was confirmed by GIWAXS and XRD (X-ray diffraction) measurements (Fig. S1(a and b)†), with the data for the guest-free **DMOF-1** system being consistent with the previously reported tetragonal *P*4/*mmm* structure (Fig. S1(c)†).[43] Considering the lattice parameters of the **DMOF-1** and Cu$_2$BDC$_2$-on-Cu(OH)$_2$
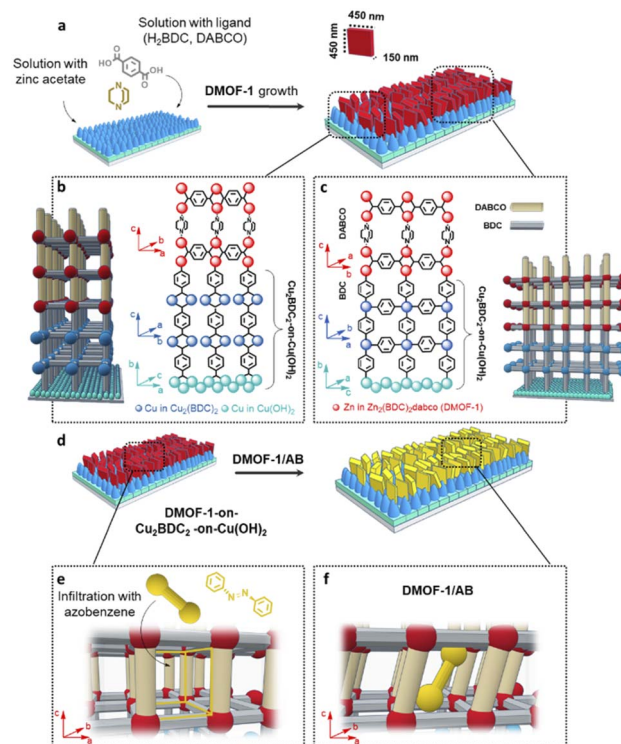

Fig. 1 Growth of DMOF-1 *via* heteroepitaxial growth and subsequent infiltration by azobenzene. (a) Synthetic scheme for the growth of the **DMOF-1** film, starting from the heteroepitaxial oriented Cu$_2$BDC$_2$-on-Cu(OH)$_2$ system. The Cu$_2$BDC$_2$-on-Cu(OH)$_2$ layer is first immersed in an ethanolic zinc acetate solution, then in the methanolic linker solution of DABCO and H$_2$BDC. (b and c) Magnified image on the interface of the heteroepitaxially grown **DMOF-1** (red cubes) on Cu$_2$BDC$_2$-on-Cu(OH)$_2$ along the parallel and perpendicular directions of Cu(OH)$_2$ nanobelts. (d) Synthetic scheme for the infiltration of **DMOF-1** films with azobenzene. (e) Schematic of the infiltration process: the azobenzene molecule enters the vacant MOF pores (yellow cubes) and (f) the flexible **DMOF-1** structure is forced to adapt to the size of the infiltrated azobenzene molecule resulting in the DMOF-1/AB assembly.

systems (Cu_2BDC_2: $P4$ space group, $a = 10.61$ Å, $b = 5.80$ Å, $c = 10.61$ Å,[38] DMOF-1: $P4/mmm$ space group, $a = 10.93$ Å, $b = 10.93$ Å, $c = 9.61$ Å),[43] we expected the crystal lattice match to occur between the a and b axes of the DMOF-1 and the Cu_2BDC_2 structure, respectively (Fig. 1(b and c)). The theoretically calculated lattice mismatch between the two MOF systems accounts for 2.9% for the a axis, and 5.7% for the b axis of the DMOF-1 system, which is in the range of epitaxial growth.[37,38,40,54] Based on X-ray data, the (100) diffraction signal of DMOF-1 was observed for the two in-plane XRD geometries with the X-ray incident angle set parallel and perpendicular to the long axis of the $Cu(OH)_2$ nanobelts (Fig. S1(a–c)†).[38] In the out-of-plane direction, the (001) diffraction signal of DMOF-1 and Cu_2BDC_2-on-$Cu(OH)_2$ is observed (Fig. S1(c)†). Hence, these findings indicate that the (h00) and (0k0) faces of the DMOF-1 structure are oriented perpendicular to the substrate. Moreover, the (100) DMOF-1 and the (100) Cu_2BDC_2 diffraction peaks show a clear angular dependence with the two maxima coinciding at 90° and 270° (Fig. S1(d and e)†). These results support our scientific hypothesis and demonstrate a crystal lattice matching between the a and b axes of DMOF-1 and Cu_2BDC_2-on-$Cu(OH)_2$ (Fig. 1(b and c)). The nascent framework grows therefore with the aid of the pillaring agent DABCO in the c axis direction with the DMOF-1 pores being available for the introduction of azobenzene as the photo-active molecule (see Fig. 1(d)).

The morphology of the DMOF-1-on-MOF film was assessed by SEM after each step of the film fabrication process. In Fig. 2, the top-view SEM images show the first MOF layer comprising oriented $Cu(OH)_2$ nanobelts (Fig. 2(a)) and after their conversion to Cu_2BDC_2 (Fig. 2(b)).[38] The growth of the DMOF-1 system on the oriented Cu_2BDC_2-on-$Cu(OH)_2$ film yields cuboid-shaped crystallites assembled as the final MOF-on-MOF film (Fig. 2(c and d)). The lateral size of the DMOF-1 crystallites was

determined to be ~450 nm with a width of ~150 nm (see the inset in Fig. 1(a)), whilst the Cu_2BDC_2-on-$Cu(OH)_2$ film accounts for ~500 nm.[38] The SEM micrographs show a preferential out-of-plane orientation of the DMOF-1 crystallites with respect to the substrate. Detailed analysis of the XRD data was performed to estimate the degree of oriented DMOF-1 crystallites (see the ESI, Fig. S2†).[55] Results showed that from the DMOF-1 crystallites a fraction of 45% is preferentially oriented towards the out-of-plane orientation with a degree of alignment of 18° as determined with the azimuthal full width half maximum of the (100) reflection in the azimuthal cut (Fig. S2(d)†).[41]

To evaluate the porosity, the DMOF-1-on-Cu_2BDC_2-on-$Cu(OH)_2$ film was deposited on a quartz crystal microbalance (QCM), where the resonance frequency change of each MOF layer was measured upon exposure to methanol vapor (Fig. S3(a)†). Owing to the porosity of the film, the DMOF-1 structure takes up significantly more methanol compared to the Cu_2BDC_2 and the bare reference crystal (Fig. S3(b)†). The methanol uptake of DMOF-1 demonstrates the pore accessibility by guest molecules. Accordingly, in the next step, we infiltrated the DMOF-1 pores with azobenzene by a vapor-phase infiltration process yielding the DMOF-1/AB film system (Fig. S4†). Considering the flexibility of the DMOF-1 structure,[34,36] we expected the DMOF-1 cage (7.5 Å × 7.5 Å) to adapt to the infiltrated azobenzene (9.0 Å) (see Fig. 1(e and f)).[28,34,36] This expected shrinkage of the DMOF-1 cage was confirmed by GIWAXS measurements and is evidenced by the splitting of the (100) reflection at $q = 5.85$ nm^{-1}, which accounts for a change of $\Delta d = 0.12$ Å in the d-spacing (Fig. 3(a and b)). This shrinkage results in the coexistence of two crystalline tetragonal phases (Fig. 3(b)), which has been previously reported to arise from the guest-induced breathing of the infiltrated DMOF-1 bulk structures.[28,34] Importantly, the orientation of the DMOF-1 layer is not lost despite a clear structural change (Fig. S5(a)†). Moreover, the position of the X-ray reflection corresponding to the Cu_2BDC_2 remains unaffected (Fig. 3(b)), which implies that although the DMOF-1 structure was rearranged, no additional stress is induced to the underlying structure.

The DMOF-1/AB crystallites comprise azobenzene molecules in the *trans*-configuration which is evidenced by the IR absorption band located at 687 cm^{-1} (Fig. 3(d)).[34] The reduced methanol uptake of azobenzene infiltrated DMOF-1 films indicates the occupation of the DMOF-1 pores with the photo-active molecules (Fig. S3(b)†).[42b] Moreover, we determined that the infiltration process can be repeated by washing the DMOF-1/AB system with ethanol to remove the azobenzene without destroying the crystallinity and orientation of the MOF structure (Fig. S5(b and c)†).

Fig. 2 SEM micrographs for the stepwise fabrication of DMOF-1 films. (a) The film preparation is performed starting from an oriented $Cu(OH)_2$ nanobelt film, (b) which is converted to Cu_2BDC_2. (c and d), Subsequent growth of DMOF-1 shows a preferential out-of-plane alignment of the crystals in the magnified image.

Time-resolved GIWAXS measurements for the photo-switching of DMOF-1/AB

To evaluate the excitation wavelengths for the photo-isomerization process, the oriented DMOF-1/AB films were purposefully grown on glass substrates to consent UV-Vis characterization. The spectra depicted in Fig. 3(e) show a continuous increase in absorbance at <400 nm, due to the introduction of additional

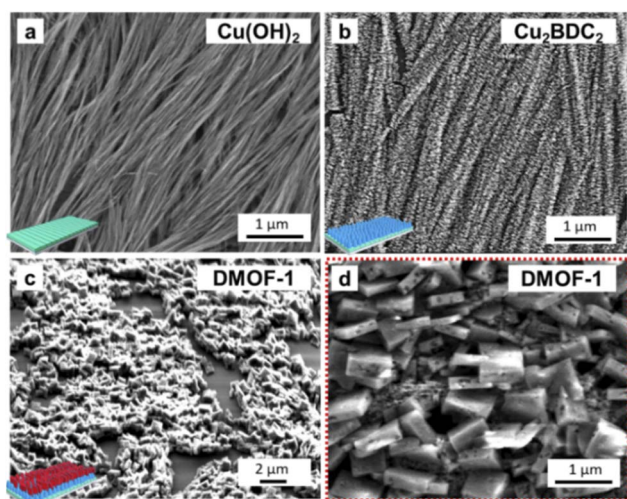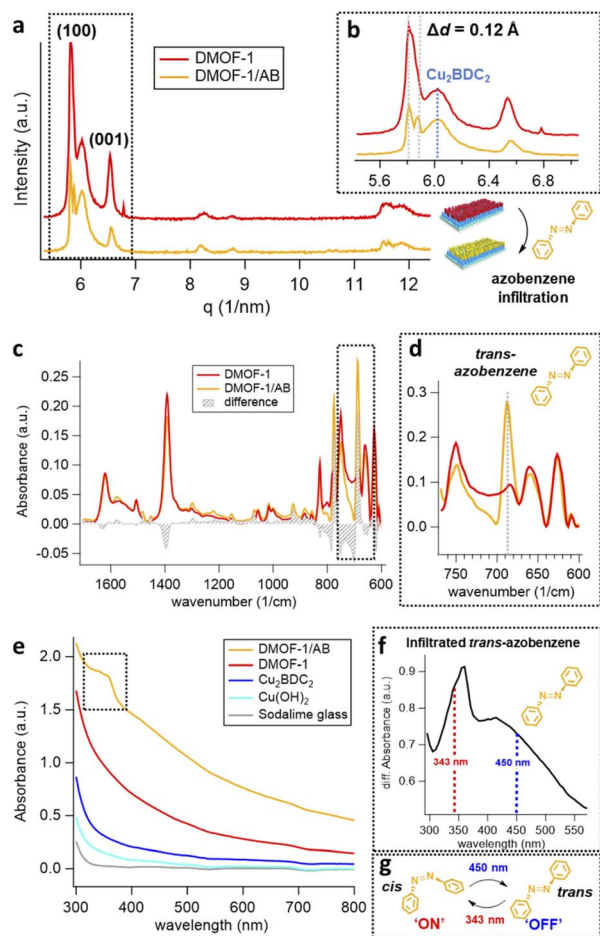Fig. 3 Characterization of the **DMOF-1/AB** films on glass substrates. (a) GIWAXS pattern of the **DMOF-1**-on-Cu_2BDC_2-on-$Cu(OH)_2$ film structure (red trace) and upon infiltration by azobenzene (yellow trace). (b) The shrinkage of the **DMOF-1** structure by $\Delta d = 0.12$ Å is not affecting the Cu_2BDC_2-on-$Cu(OH)_2$ system. (c) ATR measurements prior and after infiltration of the **DMOF-1** film show the presence of *trans*-azobenzene as indicated by the (d) intense infrared band at 687 cm^{-1}. (e) UV/Vis absorbance spectra of the **DMOF-1/AB** film system comprising (from bottom to top), the substrate (sodalime glass), $Cu(OH)_2$ nanobelts, their conversion to Cu_2BDC_2, **DMOF-1** and the infiltrated **DMOF-1/AB**. (f) Differential absorption spectrum of the infiltrated azobenzene in **DMOF-1/AB** with the absorption band of the $\pi-\pi^*$ electronic transition located at ~360 nm and the n$-\pi^*$ electronic transition at ~420 nm. The dotted lines mark the wavelengths used to photo-switch the infiltrated azobenzene (g) between its *cis*-isomer in the ON state (343 nm) and the *trans*-conformer in the OFF state (450 nm).

metal-nodes when assembling the **DMOF-1/AB**-on-Cu_2BDC_2-on-$Cu(OH)_2$ system.[30] The absorption spectrum of the infiltrated azobenzene provided in Fig. 3(f) comprises a broad absorption band located at ~350 nm ($\pi-\pi^*$ transition) and one very weak band around ~440 nm (n$-\pi^*$ transition), which is consistent with the *trans*-azobenzene in solution (Fig. S6†).[2,33] Hence, to successfully trigger the photo-switch of the azobenzene molecule, we prosecuted the forward switch (*trans*-to-*cis*, ON) with an excitation wavelength of 343 nm, and reversed the photo-switch (*cis*-to-*trans*, OFF) with 450 nm (Fig. 3(g)).

To track the time-resolved structural changes of the **DMOF-1/AB** system during the photo-switching experiments, we performed GIWAXS measurements as schematically depicted in Fig. 4(a) and the protocol outlined in Fig. 4(b). In the beginning ($t \sim 0$ s), the **DMOF-1/AB** structure is relaxed and the infiltrated azobenzene is in its *trans*-configuration (OFF). Upon excitation with 343 nm, the isomerization of the chromophore to its *cis* conformer is provoked (forward switch) and consequently, **DMOF-1/AB** converts to the ON state. Relaxation of the structure when exposed to 450 nm is initiated by the re-isomerization of azobenzene, and the OFF state is reached again (backward switch, see Fig. 3(g)). Typically, one photo-switch requires 100 s to reach the steady state, and to demonstrate the stability of the system we have repeated the ON/OFF photo-switch for 7 cycles. Between the OFF and ON state, we found that the most pronounced changes occurred for the (001) reflection (upper inset, Fig. 5(a)), which implies that the **DMOF-1** cage moves in the direction of the pillaring DABCO linker.[28] This property is supported by polarization-angle dependent absorption measurements[39] at 343 nm wavelength, as the *cis*-azobenzene molecules were found to align preferentially along the **DMOF-1** *c*-axis direction (Fig. S7†). Hence, the photo-switch results mainly in a structural change along the *c*-axis direction (inset, Fig. 5(a)), which is further confirmed by the lack of significant structural changes in the in-plane direction (Fig. S8†). Closer inspection of the (001) reflection in the out-of-plane direction shows its downshift by $\Delta q = 0.013$ nm^{-1} between the OFF and ON state which channels a structural change by $\Delta d = 0.02$ Å (Fig. S9(a)†). This is due to the larger *trans*-azobenzene molecule (9.0 Å) compared to its *cis*-conformer (5.5 Å),[8] which urges the **DMOF-1** pores to adapt between the two configurations (see schematics in Fig. 5(a)). Moreover, the structural stability of the crystalline **DMOF-1/AB** structure throughout the photo-cycling is confirmed as all reflections were found to remain unaltered over the entire experiment.

To deduce the switching kinetics of **DMOF-1/AB**, we performed exponential fits on the integrated intensity of the (001) reflection for the forward and backward switch (Fig. 5(b), inset), which are expressed as

$$I(t) = \pm A_{OFF,ON} \times \exp\left(-\frac{(t - t_{OFF,ON})}{\tau_{OFF,ON}}\right) + y_{OFF,ON}$$

where t is the time scale, $t_{OFF,ON}$ denotes the starting time of the various ON and OFF-switch events and $\tau_{OFF,ON}$ represents the decay constant. The amplitudes of $I(t)$ for the ON and OFF states are described by $+A_{ON}$ and $-A_{OFF}$, with $y_{OFF,ON}$ indicating the background off-sets. We propose that one exponential term is sufficient to model the **DMOF-1/AB** response during its ON/OFF cycling, due to the unconstrained photo-switching behavior of azobenzene in the MOF pores.[34,56,57] We exclude any structural changes arising from either the non-infiltrated **DMOF-1** structure, the pristine or the azobenzene-infiltrated Cu_2BDC_2-on-$Cu(OH)_2$ layer, as these structures revealed no changes when exposed to UV light (343 nm, Fig. S10(a–d)†). This behavior confirms that the underlying lattice is both non-responsive and/or too rigid for the photo-isomerization of azobenzene.[57] To deduce the switching constants for the ON and OFF state, we
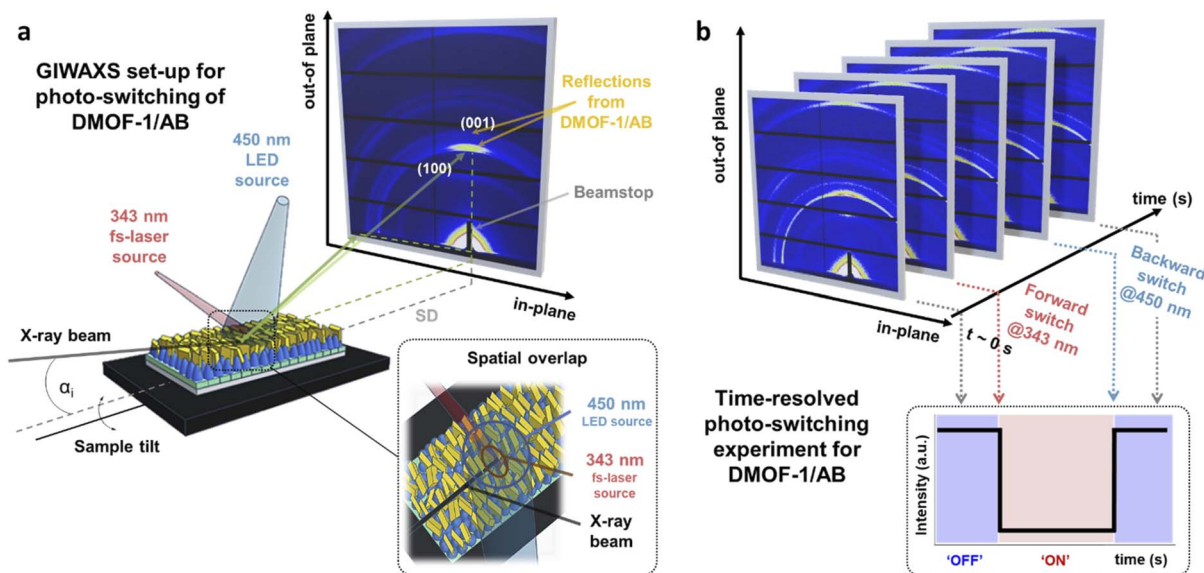
Fig. 4 Time-resolved GIWAXS measurements. (a) Schematic GIWAXS set-up for the photo-switching of **DMOF-1/AB** film structures with the sample-to-detector distance (SD) chosen to track the time-resolved evolution of the (100) and (001) reflections. Spatial overlap of the synchrotron X-ray beam with the excitation light sources for the forward (343 nm) and back isomerization (450 nm) is depicted in the inset. (b) Experimental protocol for the **DMOF-1/AB** photo-switching, where at $t \sim 0$ s **DMOF-1/AB** is relaxed (OFF). Photoexcitation with 343 nm light radiation (time zero, t_{ON}) induces the forward switch (ON) and is evidenced by a sudden drop in the scattering intensity due to the structural changes of **DMOF-1/AB**. Back-switching of the structure to OFF is performed by excitation with 450 nm (time zero, t_{OFF}), which is accompanied by an increase in the scattered intensity to the initial state (see the inset).

evaluated 6 switching cycles of the **DMOF-1/AB** structure for reproducible measurements (Fig. 5(b)). Hence, we obtained a time constant of $\tau_{ON} = 6.8$ s $\pm$ 0.7 s, when switching the **DMOF-1/AB** structure to the ON state (Fig. 5(c)). Interestingly, the initial switch to the ON state (Fig. 5(b), $t = 0$–100 s) was found to be slightly slower ($\tau_{ON} = 7.9$ s $\pm$ 0.6 s). This property was reported to occur in azobenzene-containing HKUST-1 films characterized by absorption measurements,[31] which for other crystalline azo-films was related to the creation of a favorable environment for the forward and back-switching process during the initial irradiation by UV light.[58] Hence this 'shaping' is accomplished during the first ON switch of the **DMOF-1/AB** system by irradiation with high-repetition UV light until the forward switching constant reaches a steady state ($t \sim 120$ s), after which the film undergoes a smooth ON to OFF transition (Fig. 5(c), cycle 0–5). The OFF state occurs with a time constant of $\tau_{OFF} = 8.6$ s $\pm$ 0.7 s (Fig. 5(c), backward switching cycle). We presume that the deviance between the time constants of the ON and OFF states arises from the 5 times higher power density of the 343 nm than the 450 nm irradiation source, which implies that the photo-switch is eventually dependent on the deposited energy.[3] The unaltered integrated intensity of the (001) reflection over the course of 14 photo-switching cycles (Fig. 5(b)) demonstrates that the photo-response of the **DMOF-1/AB** film structure is fully reversible and shows no significant signs of degradation of the system (see Fig. S9(b)†). Considering the entire switching process, the isomerization of azobenzene and the adaptation of the host structure are strongly dependent on the surrounding conditions.[5,59]

The initial photo-excitation process is evoked by the electronic transitions of the chromophore upon UV exposure, which typically occurs on the time scale of ~ 1 ps.[60] The structural changes related to the photo-isomerization of azobenzene in solvents were reported to require 0.5–1 ps,[60,61] and up to 180–190 ps[62] or even seconds in liquid crystals.[63] However, photoswitching in solid azobenzene systems such as functionalized azo-adlayers on Au-surfaces strongly decelerates the switch and was found to require 16 s,[64] whilst azobenzene-based films that undergo a photo-induced structural phase transition from crystalline to a disordered system switch on the time-scale of ~ 220 s.[56] In comparison, the photo-response of the herein proposed **DMOF-1/AB** film experiences one full switching cycle within 15 s (ON/OFF), which is one of the fastest observed structural transitions for azobenzene-containing solid crystalline films[56,64,65] and one of the first for structurally photoswitchable MOF films.[25,26,30–33,66]

Moreover, in relation to the bulk **DMOF-1/AB** system which was reported to require >300 min for its structural change,[34,36] preparation of **DMOF-1/AB** in oriented films accelerated this process by 3 orders of magnitude (see Fig. S11† for bulk **DMOF-1/AB** experiments). These findings imply that the fabrication of crystalline and oriented film structures is the key for the successful and fast photo-switching in solids, which we hypothesize to arise from the improved light penetration in the MOF film system.[3]

Infrared measurements on the photo-switched structures. To evidence the photo-isomerization behavior of the infiltrated azobenzene molecules throughout the **DMOF-1/AB** photocycling, infrared measurements were performed for the ON
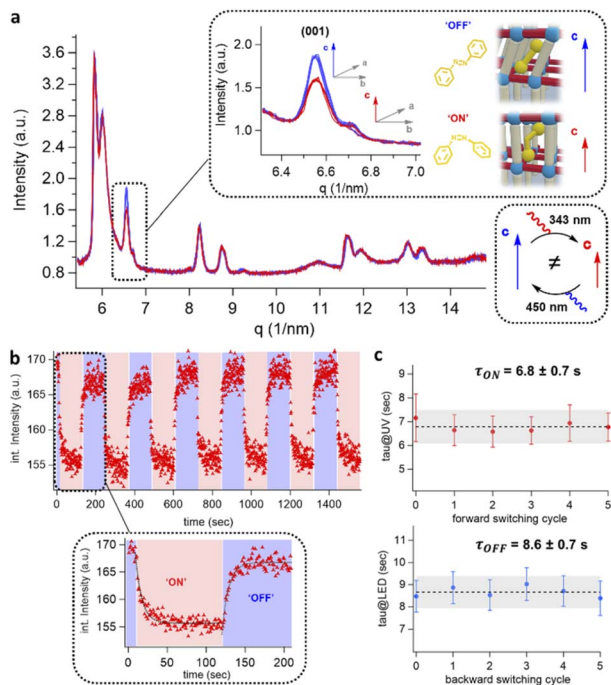
Fig. 5 Solid-state photo-switching of the **DMOF-1/AB** system by time-resolved photoexcitation GIWAXS measurements. (a) GIWAXS radial integrated data of the OFF **DMOF-1/AB** structure (blue traces) and the ON structure (red traces) on glass substrates. The inset displays the (001) reflection corresponding to the *c* lattice axis with the most prominent structural changes. (b) The **DMOF-1/AB** structure was reversibly cycled between the OFF and ON state. The change in peak intensity of the (001) reflection is displayed as integrated intensity as a function of time. The black lines in the inset are the fitting functions to evaluate the switching kinetics. (c) Forward switching to the ON state at 343 nm with an average time constant $\tau_{ON} = 6.8 \pm 0.7$ s and backward switching to the OFF state at 450 nm with an average time constant $\tau_{OFF} = 8.6 \pm 0.7$ s.

and OFF state, respectively (Fig. 6). Excitation by the 343 nm light led to the photo-isomerization of azobenzene from its *trans* (687 cm^{-1}) to the *cis*-conformer within the **DMOF-1/AB**

pores and is clearly envisioned by the infrared band located at 697 cm^{-1} in the ON state (Fig. 6(a)). Merely a portion of the infiltrated azobenzene molecules is not photo-active (9%, Fig. 6(b)).

The freshly infiltrated **DMOF-1/AB** films comprise *trans*-azobenzene within the MOF pores (*vide supra*). However, the first photo-isomerization cycle of azobenzene within the **DMOF-1/AB** pores (ON/OFF) was found to prevent the azobenzene molecules from fully reversing to their initial *trans*-conformer (Fig. S12†). Repetition of the photo-cycling experiment revealed an irreversibly 'trapped' portion of *cis*-azobenzene molecules being present in the relaxed OFF state (Fig. 6(a)). In the OFF state, the **DMOF-1/AB** film structure reaches a *trans*/*cis*-azobenzene ratio of 0.70. Comparing the ON to the OFF state, the two *cis*-azobenzene absorption bands comprise a red-shift of $\Delta\nu = 2$ cm^{-1} (Fig. 6(b)).[67] Similarly, the strong C–O vibration[68] arising from the carboxylate in the **DMOF-1** structure is shifted by $\Delta\nu = 8$ cm^{-1} (Fig. S9(d)†).[69] This property points to a strong interaction between the **DMOF-1** cage and the infiltrated azobenzene molecules.[36] Interestingly, for poorly oriented **DMOF-1/AB** films almost no shift of the vibrational bands was found to arise between the ON and the OFF switch (Fig. S13†). This property indicates the importance of fabricating an oriented **DMOF-1/AB** film structure as the concomitant interactions seem to be crucial for the progress of the photo-switch.[16]

Based on this, we presume that the initial *trans*-to-*cis* azobenzene isomerization already leads to the full structural change of the oriented **DMOF-1/AB** film system. During the initial azobenzene isomerization the interactions between the **DMOF-1** cage and the infiltrated azobenzene molecules are weakened, provoking adjacent azobenzene molecules to isomerize whilst the **DMOF-1** structure has already switched to the ON state.[36] The switching process can therefore be described by a 'cooperative movement' of the oriented **DMOF-1/AB** crystallites, which would correlate with the seconds-time scale that is required to switch the system.[16,23] To account for the origin of the strained *cis*-azobenzene molecules, we increased the power density of the 343 nm light source from 1.2 to 95 mW cm^{-2} to
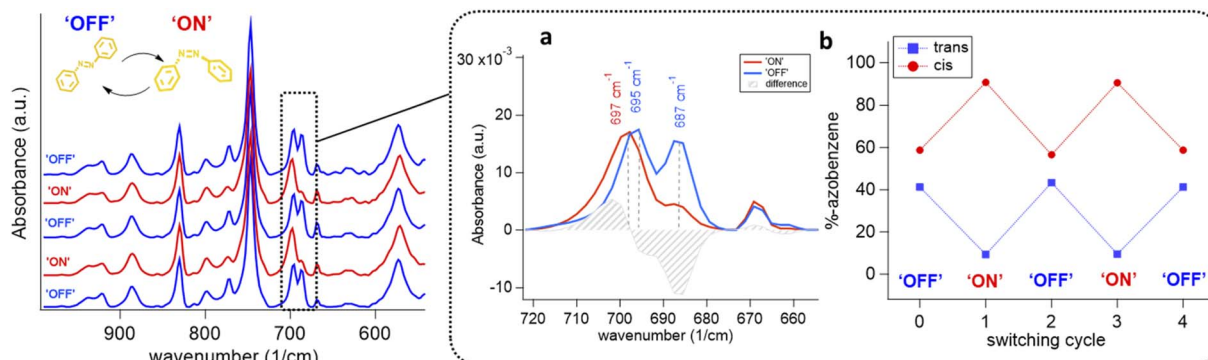

Fig. 6 Infrared measurements on the photo-switched structures. Infrared spectra of the oriented **DMOF-1/AB** films switched repeatedly from OFF (blue trace) to ON (red trace). (a) Inset displays the infiltrated azobenzene when in *trans* (blue) and *cis*-configuration (red) with a shift of $\Delta\nu = 2$ cm^{-1}. (b) The active photo-switchable azobenzene portion between the ON and the OFF state was determined from infrared measurements to account for 40% of the infiltrated azobenzene. The ON and OFF cycling as a function of the azobenzene percentage supports the reversible switching behavior.

understand if the *cis*/*trans* ratio would change (Fig. S14†). However, independent of the photon power density the portion of photo-active azobenzene molecules in the **DMOF-1** pores remained unchanged, which accounts for ~40% (Fig. 6(b)). This percentage is comparable to the *cis*-portion reported for bulk **DMOF-1/AB** systems[28,34] and is eventually an intrinsic property of the system that can be attributed to the loading level of one azobenzene molecule per **DMOF-1** pore, which is the estimated loading for the **DMOF-1/AB** films (see the ESI†).[28,31,36]

However, the presence of azobenzene molecules frozen in the *cis*-configuration is still unclear, since no correlation between the film preparation conditions or chemical parameters could be established.[31] As a comparison, this behavior was not reported for the isostructural well-oriented yet non-flexible Cu_2BDC_2DABCO system when using $Cu(OH)_2$ nanobelts.[39] Based on this, we presume that these irreversibly 'trapped' molecules are both a consequence of the interaction of the azobenzene molecule with the **DMOF-1** cage[28,31,36] and the considerable lattice mismatch between the **DMOF-1** and the Cu_2BDC_2-on-$Cu(OH)_2$ structure (*vide supra*). This property eventually creates 'strained' **DMOF-1** pores, which trap these in their *cis*-conformation upon azobenzene infiltration thus inhibiting the backward relaxation due to a better stabilization of the *cis*-isomer.[28] Therefore, the ON-to-OFF switching characteristics of the **DMOF-1/AB** film are mainly related to the interactions arising between the MOF cage and the infiltrated azobenzene molecules,[28,31,36] as well as to the degree of azobenzene loading.[23,28,36] In addition, the influence of the total **DMOF-1**-Cu_2BDC_2-on-$Cu(OH)_2$ film thickness is another crucial parameter to assess, which will be the scope of future research. Nevertheless, IR data (Fig. 6(b)) support the reversibility of the photo-switching process and verify that the crystalline **DMOF-1** structure responds to the photo-switch of the azobenzene.

Conclusions

This paper demonstrates an experimental strategy to characterize and quantify the time-resolved structural transformations by time-resolved GIWAXS measurements, as outlined on the herein employed photo-switchable **DMOF-1/AB**-on-Cu_2BDC_2-on-$Cu(OH)_2$ oriented film system. The described set-up involves two light sources of 343 and 450 nm wavelengths, which triggered the isomerization of azobenzene within the **DMOF-1** pores that was found to provoke a strong structural response along the *c* axis of the **DMOF-1** structure. As further evidenced by infrared spectroscopic measurements, strong interactions within the oriented film system promoted the **DMOF-1** film structure to cooperatively switch within 15 s for one ON/OFF cycle. In comparison to the bulk system, the herein fabricated oriented **DMOF-1/AB** film was found to accelerate the photo-switching process from hours to the seconds-scale, being moreover reversible and free of fatigue for several switching repetitions. The photo-switching of the oriented **DMOF-1/AB** film was shown to be one of the fastest observed structural transitions for azobenzene-containing solid crystalline films, and one of the first for photo-switchable MOF films. With the herein selected approach to design photo-switchable MOF films together with the employed methodology we aim to introduce a general conceptual advance towards 4D-MOFs to assess the photo-responsive behavior of similar or even more advanced solid film systems.

Data availability

Experimental data have been provided in the ESI.†

Author contributions

H. A., P. F. and S. K. conceived and designed the project. S. K. carried out most of the experimental work including the optimization and fabrication of the system and wrote the manuscript. D. N. and B. M. assisted with the data analysis and completed the GIWAXS measurements with S. K., S. D.-Z. provided some starting materials and performed SEM imaging. G. B. completed the infrared measurements. F. C. and M. L.-M. completed the XRD measurements, whilst R. K. conducted the QCM measurements.

Conflicts of interest

There are no conflicts to declare.

Acknowledgements

Notes and references

1 A. Gonzalez, E. S. Kengmana, M. V. Fonseca and G. Han, *Mater. Today Adv.*, 2020, **6**, 100058.

2 A. Goulet-Hanssens, F. Eisenreich and S. Hecht, *Adv. Mater.*, 2020, **32**, e1905966.

3 R. Haldar, L. Heinke and C. Wöll, *Adv. Mater.*, 2020, **32**, e1905227.

4 E. Moulin, L. Faour, C. C. Carmona-Vargas and N. Giuseppone, *Adv. Mater.*, 2020, **32**, e1906036.

5 A. B. Grommet, L. M. Lee and R. Klajn, *Acc. Chem. Res.*, 2020, **53**, 2600.

6 S. Horike, S. Shimomura and S. Kitagawa, *Nat. Chem.*, 2009, **1**, 695.

7 Z. Chang, D.-H. Yang, J. Xu, T.-L. Hu and X.-H. Bu, *Adv. Mater.*, 2015, **27**, 5432.

8 F. Bigdeli, C. T. Lollar, A. Morsali and H.-C. Zhou, *Angew. Chem., Int. Ed.*, 2020, **59**, 4652.

9 W. Cai, J. Wang, C. Chu, W. Chen, C. Wu and G. Liu, *Adv. Sci.*, 2019, **6**, 1801526.

10 L. Vanduyfhuys, S. M. J. Rogge, J. Wieme, S. Vandenbrande, G. Maurin, M. Waroquier and V. van Speybroeck, *Nat. Commun.*, 2018, **9**, 204.

11 S. Bureekaew, S. Amirjalayer and R. Schmid, *J. Mater. Chem.*, 2012, **22**, 10249.

12 S. Henke, A. Schneemann, A. Wütscher and R. A. Fischer, *JACS*, 2012, **134**, 9464.

13 S.-Q. Wang, S. Mukherjee and M. J. Zaworotko, *Faraday Discuss.*, 2021, **231**, 9.

14 Z. Liu, L. Zhang and D. Sun, *Chem. Commun.*, 2020, **56**, 9416.

15 S. Kitagawa and M. Kondo, *Bull. Chem. Soc. Jpn.*, 1998, **71**, 1739.

16 S. Ehrling, H. Miura, I. Senkovska and S. Kaskel, *Trends in Chem.*, 2021, **3**, 291.

17 A. E. Hoffman, J. Wieme, S. M. Rogge, L. Vanduyfhuys and V. van Speybroeck, *Cryst. Mater.*, 2019, **234**, 529.

18 A. U. Ortiz, A. Boutin and F.-X. Coudert, *Chem. Commun.*, 2014, **50**, 5867.

19 (*a*) J. Liu, L. Chen, H. Cui, J. Zhang, L. Zhang and C.-Y. Su, *Chem. Soc. Rev.*, 2014, **43**, 6011; (*b*) J. H. Lee, S. Jeoung, Y. G. Chung and H. R. Moon, *Coord. Chem. Rev.*, 2019, **389**, 161; (*c*) H. Furukawa, K. E. Cordova, M. O'Keeffe and O. M. Yaghi, *Science*, 2013, **341**, 1230444; (*d*) A. M. Rice, C. R. Martin, V. A. Galitskiy, A. A. Berseneva, G. A. Leith and N. B. Shustova, *Chem. Rev.*, 2020, **120**, 8790.

20 É. Whelan, F. W. Steuber, T. Gunnlaugsson and W. Schmitt, *Coord. Chem. Rev.*, 2021, **437**, 213757.

21 N. D. Shepherd and D. M. D'Alessandro, *Chem. Phys. Rev.*, 2021, **2**, 11301.

22 J. D. Evans, V. Bon, I. Senkovska, H.-C. Lee and S. Kaskel, *Nat. Commun.*, 2020, **11**, 2690.

23 J. Nishida, A. Tamimi, H. Fei, S. Pullen, S. Ott, S. M. Cohen and M. D. Fayer, *PNAS*, 2014, **111**, 18442.

24 A. B. Kanj, K. Müller and L. Heinke, *Macromol. Rapid Commun.*, 2018, **39**, 1700239.

25 X. Yu, Z. Wang, M. Buchholz, N. Füllgrabe, S. Grosjean, F. Bebensee, S. Bräse, C. Wöll and L. Heinke, *PCCP*, 2015, **17**, 22721.

26 D. Mutruc, A. Goulet-Hanssens, S. Fairman, S. Wahl, A. Zimathies, C. Knie and S. Hecht, *Angew. Chem., Int. Ed.*, 2019, **58**, 12862.

27 H. Huang, H. Sato and T. Aida, *JACS*, 2017, **139**, 8784.

28 K. Griffiths, N. R. Halcovitch and J. M. Griffin, *Chem. Mater.*, 2020, **32**, 9925.

29 A. Modrow, D. Zargarani, R. Herges and N. Stock, *Dalton Trans.*, 2011, **40**, 4217.

30 K. Müller, J. Wadhwa, J. Singh Malhi, L. Schöttner, A. Welle, H. Schwartz, D. Hermann, U. Ruschewitz and L. Heinke, *Chem. Commun.*, 2017, **53**, 8070.

31 T. Koehler, I. Strauss, A. Mundstock, J. Caro and F. Marlow, *J. Phys. Chem. Lett.*, 2021, **12**(36), 8903–8908.

32 Z. Wang, K. Müller, M. Valášek, S. Grosjean, S. Bräse, C. Wöll, M. Mayor and L. Heinke, *J. Phys. Chem. C*, 2018, **122**, 19044.

33 K. Müller, A. Knebel, F. Zhao, D. Bléger, J. Caro and L. Heinke, *Chemistry*, 2017, **23**, 5434.

34 N. Yanai, T. Uemura, M. Inoue, R. Matsuda, T. Fukushima, M. Tsujimoto, S. Isoda and S. Kitagawa, *JACS*, 2012, **134**, 4501.

35 Y. Kim, R. Haldar, H. Kim, J. Koo and K. Kim, *Dalton Trans.*, 2016, **45**, 4187.

36 M. Rödl, S. Kerschbaumer, H. Kopacka, L. Blaser, F. R. S. Purtscher, H. Huppertz, T. S. Hofer and H. A. Schwartz, *RSC Adv.*, 2021, **11**, 3917.

37 K. Ikigaki, K. Okada and M. Takahashi, *ACS Appl. Nano Mater.*, 2021, **4**, 3467.

38 P. Falcaro, K. Okada, T. Hara, K. Ikigaki, Y. Tokudome, A. W. Thornton, A. J. Hill, T. Williams, C. Doonan and M. Takahashi, *Nat. Mater.*, 2017, **16**, 342.

39 K. Okada, M. Nakanishi, K. Ikigaki, Y. Tokudome, P. Falcaro, C. J. Doonan and M. Takahashi, *Chem. Sci.*, 2020, **11**, 8005.

40 (*a*) K. Ikigaki, K. Okada, Y. Tokudome, T. Toyao, P. Falcaro, C. J. Doonan and M. Takahashi, *Angew. Chem., Int. Ed.*, 2019, **58**, 6886; (*b*) K. Ikigaki, K. Okada and M. Takahashi, *ACS Appl. Nano Mater.*, 2021, **4**, 3467–3475; (*c*) T. Stassin, S. Rodríguez-Hermida, B. Schrode, A. Cruz, F. Carraro, D. Kravchenko, V. Creemers, I. Stassen, T. Hauffman, D. De Vos, et al., *Chem. Commun.*, 2019, **55**, 10056–10059.

41 M. Linares-Moreau, L. A. Brandner, T. Kamencek, S. Klokic, F. Carraro, K. Okada, M. Takahashi, E. Zojer, C. J. Doonan and P. Falcaro, *Adv. Mater. Interfaces*, 2021, **8**, 2101039.

42 (*a*) D. Das and H. Agarkar, *ACS Omega*, 2018, **3**, 7630; (*b*) N. Prasetya and B. Ladewig, *ACS Appl. Mater. Interfaces*, 2018, **10**, 34291–34301.

43 D. N. Dybtsev, H. Chun and K. Kim, *Angew. Chem., Int. Ed.*, 2004, **43**, 5033.

44 R. Klajn, *Pure Appl. Chem.*, 2010, **82**, 2247.

45 (*a*) K. Titov, Z. Zeng, M. R. Ryder, A. K. Chaudhari, B. Civalleri, C. S. Kelley, M. D. Frogley, G. Cinque and J.-C. Tan, *J. Phys. Chem. Lett.*, 2017, **8**, 5035; (*b*) B. Pattengale, S. Ostresh, C. A. Schmuttenmaer and J. Neu, *Chem. Rev.*, 2022, **122**, 132.

46 C. L. Hobday, R. J. Marshall, C. F. Murphie, J. Sotelo, T. Richards, D. R. Allan, T. Düren, F.-X. Coudert, R. S. Forgan, C. A. Morrison, et al., *Angew. Chem., Int. Ed.*, 2016, **55**, 2401.

47 S. Devautour-Vinot, G. Maurin, F. Henn, C. Serre, T. Devic and G. Férey, *Chem. Commun.*, 2009, 2733.

48 (*a*) M. Burian, B. Marmiroli, A. Radeticchio, C. Morello, D. Naumenko, G. Biasiol and H. Amenitsch, *J. Synchrotron Rad.*, 2020, **27**, 51; (*b*) H. Amenitsch, M. Rappolt, M. Kriechbaum, H. Mio, P. Laggner and S. Bernstorff, *J. Synchrotron Rad.*, 1998, **5**, 506.

49 (*a*) A. Hexemer and P. Müller-Buschbaum, *IUCrJ*, 2015, **2**, 106; (*b*) M. Pflüger, V. Soltwisch, J. Probst, F. Scholze and M. Krumrey, *IUCrJ*, 2017, **4**, 431.

50 N. Kavoosi, V. Bon, I. Senkovska, S. Krause, C. Atzori, F. Bonino, J. Pallmann, S. Paasch, E. Brunner and S. Kaskel, *Dalton Trans.*, 2017, **46**, 4685.

51 (*a*) F. Ercole, T. P. Davis and R. A. Evans, *Polym. Chem.*, 2010, **1**, 37; (*b*) Z. G. Fthenakis, Z. Zhu, D. Teich, G. Seifert and

D. Tománek, *Phys. Rev. B: Condens. Matter Mater. Phys.*, 2013, **88**, 245402; (*c*) Y. Jiang and L. Heinke, *Langmuir*, 2021, **37**, 2.

52 R. Lyndon, K. Konstas, B. P. Ladewig, P. D. Southon, C. J. Kepert and M. R. Hill, *Angew. Chem., Int. Ed.*, 2013, **52**, 3695.

53 S. Castellanos, F. Kapteijn and J. Gascon, *CrystEngComm*, 2016, **18**, 4006.

54 Z. Wang, J. Liu, B. Lukose, Z. Gu, P. G. Weidler, H. Gliemann, T. Heine and C. Wöll, *Nano Lett.*, 2014, **14**, 1526.

55 (*a*) L. Oesinghaus, J. Schlipf, N. Giesbrecht, L. Song, Y. Hu, T. Bein, P. Docampo and P. Müller-Buschbaum, *Adv. Mater. Interfaces*, 2016, **3**, 1600403; (*b*) Z. Jiang, *J. Appl. Crystallogr.*, 2015, **48**, 917.

56 C. Weber, L. Pithan, A. Zykov, S. Bommel, F. Carla, R. Felici, C. Knie, D. Bléger and S. Kowarik, *J. Phys. Condens. Mater.*, 2017, **29**, 434001.

57 H. A. Schwartz, U. Ruschewitz and L. Heinke, *Photochem. Photobiol. Sci.*, 2018, **17**, 864.

58 Z.-F. Liu, B. H. Loo, R. Baba and A. Fujishima, *Chem. Lett.*, 1990, **19**, 1023.

59 L. Pesce, C. Perego, A. B. Grommet, R. Klajn and G. M. Pavan, *JACS*, 2020, **142**, 9792.

60 T. Fujino, S. Y. Arzhantsev and T. Tahara, *J. Phys. Chem. A*, 2001, **105**, 8123.

61 I. K. Lednev, T.-Q. Ye, P. Matousek, M. Towrie, P. Foggi, F. Neuwahl, S. Umapathy, R. E. Hester and J. N. Moore, *Chem. Phys. Lett.*, 1998, **290**, 68.

62 M. Hada, D. Yamaguchi, T. Ishikawa, T. Sawa, K. Tsuruta, K. Ishikawa, S.-Y. Koshihara, Y. Hayashi and T. Kato, *Nat. Commun.*, 2019, **10**, 4159.

63 M. L. Rahman, S. M. Sarkar, M. M. Yusoff, S. Kumar and C. Tschierske, *RSC Adv.*, 2015, **5**, 87019.

64 U. Jung, C. Schütt, O. Filinova, J. Kubitschke, R. Herges and O. Magnussen, *J. Phys. Chem. C*, 2012, **116**, 25943.

65 (*a*) I. V. Malyar, E. Titov, N. Lomadze, P. Saalfrank and S. Santer, *J. Chem. Phys.*, 2017, **146**, 104703; (*b*) A. Khayyami, A. Philip, J. Multia and M. Karppinen, *Dalton Trans.*, 2020, **49**, 11310; (*c*) E. Sundin, F. Johansson, V. Saavedra Becerril, J. Wallenstein, A. Gasslander, J. Mårtensson and M. Abrahamsson, *Mater. Adv.*, 2021, **2**, 2328.

66 L. Heinke, M. Cakici, M. Dommaschk, S. Grosjean, R. Herges, S. Bräse and C. Wöll, *ACS Nano*, 2014, **8**, 1463.

67 D. Hermann, H. A. Schwartz, M. Werker, D. Schaniel and U. Ruschewitz, *Chem.–Eur. J.*, 2019, **25**, 3606.

68 H. Nabipour, B. Soltani and N. Ahmadi Nasab, *J. Inorg. Organomet. Polym.*, 2018, **28**, 1206.

69 (*a*) J. Wieme, S. M. J. Rogge, P. G. Yot, L. Vanduyfhuys, S.-K. Lee, J.-S. Chang, M. Waroquier, G. Maurin and V. van Speybroeck, *J. Mater. Chem. A*, 2019, **7**, 22663; (*b*) A. E. J. Hoffman, L. Vanduyfhuys, I. Nevjestić, J. Wieme, S. M. J. Rogge, H. Depauw, P. van der Voort, H. Vrielinck and V. van Speybroeck, *J. Phys. Chem. C*, 2018, **122**, 2734.